
Research Article: New Research | Novel Tools and Methods

The impact of chemical fixation on the microanatomy of mouse organotypic hippocampal slices

<https://doi.org/10.1523/ENEURO.0104-23.2023>

Cite as: eNeuro 2023; 10.1523/ENEURO.0104-23.2023

Received: 26 March 2023

Revised: 26 July 2023

Accepted: 28 July 2023

This Early Release article has been peer-reviewed and accepted, but has not been through the composition and copyediting processes. The final version may differ slightly in style or formatting and will contain links to any extended data.

Alerts: Sign up at www.eneuro.org/alerts to receive customized email alerts when the fully formatted version of this article is published.

Copyright © 2023 Idziak et al.

This is an open-access article distributed under the terms of the Creative Commons Attribution 4.0 International license, which permits unrestricted use, distribution and reproduction in any medium provided that the original work is properly attributed.

1 **The impact of chemical fixation on the microanatomy of mouse organotypic**
2 **hippocampal slices**

3 **Abbreviated title:** Anatomical impact of PFA fixation on brain tissue

4 Agata Idziak¹, V.V.G. Krishna Inavalli¹, Stephane Bancelin¹, Misa Arizono^{1,2*}, U.
5 Valentin Nägerl^{1*}

6 ¹ Univ. Bordeaux, CNRS, IINS, UMR 5297, F-33000 Bordeaux, France

7 ² Department of Pharmacology, Kyoto University Graduate School of Medicine/The
8 Hakubi Center for Advanced Research, Kyoto University

9 *Co-corresponding authors (arizono.misa.7s@kyoto-u.ac.jp and valentin.nagerl@u-
10 bordeaux.fr)

11 **Number of pages:** 21

12 **Number of figures:** 4

13 **Number of tables:** 1

14 **Number of words:** **Abstract (235), Introduction (663), Discussion (734)**

15 **Conflict of interest statement:** The authors declare no competing financial interests.

16 **Acknowledgments:** This work was supported by grants to UVN from the ANR (ERA
17 NET NEURON, ANR-17-NEU3-0005, ANR-17-CE37-0011), Fondation pour la
18 Recherche Médicale, Human Frontier Science Program (RGP0041/2019), European
19 Research Council Synergy grant (ENSEMBLE, #951294 to UVN) and a PhD fellowship
20 from Bordeaux Neurocampus Graduate Program (to AI). SB received funding from
21 Horizon 2020 program under the Marie Skłodowska-Curie Grant #794492, as well as
22 from the Fonds AXA pour la Recherche, AXA Banque Direction Banque Patrimoniale et
23 ses donateurs. MA received funding from Japan Society for the Promotion of Science
24 (JSPS). The authors thank R. Sterling for preparing PFA solutions, constructing sample
25 holder and ensuring safety measurements for handling PFA solutions. We thank F.
26 Quici, J. Angibaud and IINS Cell Culture Facility for support with organotypic slice
27 cultures. We thank A. Boyce and Y. Dembitskaya for comments on the manuscript.

28 **Author contributions:** AI carried out all experiments and analysis. MA provided
29 supervision, technical and intellectual input. VVGKI and SB provided technical support
30 for the STED microscopy. UVN conceived the study and provided supervision. The
31 paper was written by AI, MA and UVN with input from all authors.

32

33

34

35

36 **Abstract**

37 Chemical fixation using paraformaldehyde (PFA) is a standard step for preserving cells
38 and tissues for subsequent microscopic analyses such as immunofluorescence or
39 electron microscopy. However, chemical fixation may introduce physical alterations in
40 the spatial arrangement of cellular proteins, organelles and membranes. With the
41 increasing use of super-resolution microscopy to visualize cellular structures with
42 nanometric precision, assessing potential artifacts - and knowing how to avoid them -
43 takes on special urgency.

44 We addressed this issue by taking advantage of live-cell super-resolution microscopy
45 that makes it possible to directly observe the acute effects of PFA on organotypic
46 hippocampal brain slices, allowing us to compare tissue integrity in a 'before-and-after'
47 experiment. We applied super-resolution shadow imaging to assess the structure of the
48 extracellular space (ECS) and regular super-resolution microscopy of fluorescently
49 labeled neurons and astrocytes to quantify key neuroanatomical parameters.

50 While the ECS volume fraction and micro-anatomical organization of astrocytes
51 remained largely unaffected by the PFA treatment, we detected subtle changes in
52 dendritic spine morphology and observed substantial damage to cell membranes. Our
53 experiments show that PFA application via immersion does not cause a noticeable
54 shrinkage of the ECS in hippocampal brain slices maintained in culture, unlike the
55 situation in transcordially perfused animals *in vivo* where the ECS typically becomes
56 nearly depleted.

57 Our study outlines an experimental strategy to evaluate the quality and pitfalls of various
58 fixation protocols for the molecular and morphological preservation of cells and tissues.

59 **Significance Statement**

60 Chemical fixation of biological samples using PFA is a standard step routinely
61 performed in neuroscience labs. However, it is known to alter various anatomical
62 parameters ranging from protein distribution to cell morphology, potentially affecting our
63 interpretation of anatomical data. With the increasing use of super-resolution
64 microscopy, understanding the extent and nature of fixation artifacts is an urgent
65 concern.

66 Here, we use live STED microscopy to monitor in real time the impact of PFA on the
67 microanatomy of organotypic hippocampal brain slices. Our results demonstrate that
68 while PFA has little impact on the extracellular space and astrocytes, it compromises
69 cell membranes and dendritic structures. Our study provides a strategy for a direct
70 characterization of fixation artifacts at the nanoscale, facilitating the optimization of
71 fixation protocols.

72 **Introduction**

73 Chemical fixation is a commonly used preservation step for electron microscopy (EM)
74 and super-resolution microscopy techniques, such as Stimulated Emission Depletion
75 microscopy (STED), single-molecule localization microscopy and expansion
76 microscopy. These techniques permit structural and molecular analyses of cells and
77 tissues at a sub-microscopic level. Chemical fixatives like paraformaldehyde (PFA)
78 covalently cross-link proteins, which has the effect of physically hardening the cellular
79 and molecular structure of the sample (Fox et al., 1985). This procedure is to protect the
80 sample from decay and damage during subsequent processing steps, such as tissue
81 slicing, dehydration or embedding in resin.

82 However, it is known that even the most carefully executed fixation protocol can
83 introduce structural artifacts that compromise data quality and interpretation (Ebersold
84 et al., 1981; Ryter, 1988; Wyffels, 2001; Schnell et al., 2012). While these problems are
85 perhaps not noticeable at a macroscopic level, they might appear at the microscopic
86 subcellular scale. Indeed, organelles such as endosomes and lysosomes become
87 deformed by chemical fixation (Murk et al., 2003), while cellular proteins can still move
88 substantially and reposition after chemical fixation, potentially casting doubts over
89 conclusions based on this approach (Tanaka et al., 2010).

90 As the spatial resolution of modern microscopy techniques keeps improving, allowing
91 researchers to make ever more detailed and discriminating observations, concerns
92 about fixation artifacts become more relevant. Recent super-resolution techniques can
93 now reach into the low nanometer range (Arizono et al., 2023), where fixation artifacts
94 may abound. In turn, these gains in spatial resolution necessitate the development of

95 more stringent ways to assess the quality of fixation protocols and how well they can
96 preserve cellular elements at this finer spatial scale.

97 The question of how much the micro-architecture and ultrastructure of brain tissue is
98 affected by chemical fixation was addressed in two EM studies that compared the
99 effects of chemical and cryogenic fixation protocols on tissue fine structure. Cryogenic
100 fixation is based on rapid high-pressure freezing of the sample, which produces
101 amorphous ice instead of ice crystals, that otherwise would destroy the ultrastructure.
102 These studies clearly showed that chemical fixation via transcardial perfusion leads to a
103 strong depletion of the extracellular space (ECS) as well as changes in astrocytic
104 (Korogod et al., 2015) and dendritic spine morphology (Tamada et al., 2020), raising
105 serious concerns about the use of chemical fixation protocols in high-resolution
106 anatomical studies of brain tissue. However, due to differences in sample preparation
107 required for either fixation method (transcardial perfusion of the brain *in vivo* with
108 buffered PFA versus rapid cryo-genic freezing of acute brain slices with subsequent
109 storage in liquid nitrogen) and the inability to compare the EM samples with their live
110 originals, the reason of the observed differences remains elusive.

111 To directly compare nanoscale neuroanatomical structures before and after chemical
112 fixation, we took advantage of the super-resolution shadow imaging (SUSHI) technique,
113 which is based on 3D-STED microscopy and fluorescence labeling of the interstitial fluid
114 (Tonnesen et al., 2018). SUSHI allows for visualization of tissue anatomy, including the
115 ECS, projecting all cellular structures as sharply contoured ‘shadows’, providing a
116 comprehensive and non-biased view of the cellular architecture of the tissue. Using this
117 technique, we imaged organotypic brain slices and analyzed the impact of PFA on the

118 ECS. In addition, we imaged fluorescently labeled astrocytes and neurons, and
119 analyzed the effect of PFA on their nanoscale morphology in a before-and-after manner.

120 We observed that PFA does not induce major changes in the shape and size of the
121 ECS and astrocytes. However, we detected subtle changes in dendritic spine
122 morphology as well as a widespread disruption of cellular membranes and cellular
123 blebbing.

124 The study gives a 'real time' and nanoscale view of the effects of PFA on tissue micro-
125 architecture of cultured hippocampal slices, revealing the extent and type of fixation
126 artifacts, which had remained inconclusive. Applying this approach to other brain areas
127 and tissue preparations (acute brain slices, intact brain *in vivo*) may help the
128 development of fixation protocols to preserve the native structure of the tissue as well
129 as possible.

130

131 **Materials and Methods**

132 **Mouse line**

133 Animal experimental procedures were in accordance with the French National Code of
134 Ethics on Animal Experimentation and approved by the Committee of Ethics of
135 Bordeaux. All procedures were performed according to the guidelines of the European
136 Directive 2010/63/UE.

137 Mice were housed under a 12 h light/12 h dark cycle at 20-22 °C with *ad libitum* access
138 to food and water in the animal facility of the Interdisciplinary Institute for Neuroscience
139 (University of Bordeaux/CNRS) and monitored daily by trained staff. All animals used

140 were free of any disease or infection at the time of experiments. Pregnant females and
141 females with litters were kept in cages with one male. We did not distinguish between
142 males and females among the perinatal pups used for organotypic cultures, as potential
143 anatomical and/or physiological differences between the two sexes were considered
144 irrelevant in the context of this study.

145 C57Bl/6J wild-type mice were used for all experiments in this study.

146 **Organotypic brain slices**

147 Organotypic hippocampal slices (Gahwiler, 1981) were dissected from 5 to 7 days old
148 mice, and were cultured for 2 to 5 weeks in a roller drum at 35°C (for details, see
149 (Tonnesen et al., 2018)). Once a week, 500 µl of medium was exchanged in the tubes.
150 For experiments, a given coverslip with a slice was mounted in an imaging chamber,
151 and the slice was imaged from below through the glass coverslip, while PFA-containing
152 solutions were added to the imaging chamber from above.

153 **Viral injections**

154 In order to fluorescently label neurons or astrocytes, we have introduced either Sindbis-
155 Citrine or AAV2/1.gfaABC1D-Clover viruses to the brain slices via microinjections using
156 a glass pipette connected to a Picospritzer (Parker Hannifin). Briefly, the virus was
157 injected via a pipette positioned into the CA1 area of the slice by brief pressure pulses
158 (30 ms; 15 psi). For imaging of the neurons, Sindbis-Citrine virus was injected into 2-
159 week old wild-type slices one day before the experiments. To image astrocytes, 2-week
160 old wild-type slices were injected with AAV2/1.gfaABC1D-Clover two weeks before the
161 experiments.

162

163 **Extracellular labeling**

164 Extracellular labeling of organotypic slices was performed as described before
165 (Tonnesen et al., 2018). In brief, once the slice was transferred to the imaging chamber,
166 it was immersed in HEPES-buffered artificial cerebrospinal fluid (ACSF), containing 200
167 μM of the fluorescent dye Calcein (Dojindo Laboratories).

168 **Chemical fixation**

169 After acquiring a live image of a slice (where either the ECS, neurons or astrocytes
170 were labeled), the Calcein/ACSF or ACSF-only solutions were carefully removed with a
171 pipette, making sure to keep drift of the slice to a minimum. Subsequently, solutions
172 containing 4% PFA diluted in HEPES-based ACSF with or without Calcein were
173 pipetted on top of the slice. To minimize the evaporation of PFA, the imaging chamber
174 was covered with a lid.

175 For overnight chemical fixation, the organotypic slices on a glass coverslip were
176 transferred from the roller drum tube to a 6-well plate and instantly immersed in 4% PFA
177 diluted in 1x PBS solution. The 6-well plate was placed at 4 °C overnight, followed by 3
178 washes in PBS. Finally, the fixed slices on the glass coverslip were mounted onto the
179 imaging chamber containing Calcein/ACSF solution.

180 **3D-STED microscopy**

181 We used a home-built 3D-STED setup (for details, see (Inavalli et al., 2019))
182 constructed around an inverted microscope body (DMI 6000 CS, Leica Microsystems),

183 which was equipped with a TIRF oil objective (100X, 1.47 NA, HXC APO, Leica
184 Microsystems) and contained within a heating box (Cube and Box, Life Imaging
185 Services) to maintain a stable temperature of 32°C. A pulsed-laser (PDL 800-D,
186 PicoQuant) was used to deliver excitation pulses (90 ps at 80 MHz) at 485 nm and a
187 synchronized de-excitation laser (Onefive Katana 06 HP, NKT Photonics) operating at
188 592 nm was used to generate the STED light pulses (500-700 ps). The STED beam
189 was reflected on a spatial light modulator (SLM, Easy3D Module, Abberior Instruments)
190 to generate a mixture of doughnut- and bottle-shaped beams for 2D and 3D-STED,
191 respectively. Image acquisition was controlled by the Inspector software (Abberior
192 Instruments). The performance and spatial resolution of the microscope was checked
193 and optimized by visualizing and overlapping the PSFs of the laser beams using 150
194 nm gold nano-spheres and 40 nm fluorescent beads and correcting the main optical
195 aberrations with the SLM. The spatial resolution was 175 nm (lateral) and 450 nm
196 (axial) in confocal mode and 60 nm (lateral) and 160 nm (axial) in STED mode.

197 **Image acquisition**

198 For imaging, slices were transferred on their glass coverslip to the imaging chamber
199 and immersed in ACSF consisting of (in mM): 119 NaCl, 2.5 KCl, 1.3 MgSO₄, 1
200 NaH₂PO₄ x 2H₂O, 2.5 CaCl₂ x 2H₂O, 20 D-Glucose x H₂O and 10 HEPES (all from
201 Sigma Aldrich); 300 mOsm; pH 7.4. We acquired confocal image stacks with the
202 following parameters: 100 x 100 x 4 μm³ with a Δz size of 1 μm and a pixel size of 48.8
203 nm. For STED imaging, we either acquired 100 x 100 μm² single sections or z-stacks
204 (15 x 15 x 1 μm³ or 25 x 25 x 1 μm³ with a Δz size of 200 nm). All STED images were
205 acquired with a pixel size of 19.53 nm and a pixel dwell time of 30 μs. The excitation

206 power was 0.5 μ W and STED power was 30 mW at the entrance pupil of the objective.
207 We adjusted the z focus and the xy stage to keep sample drift to a minimum between
208 image acquisitions. Images were cropped at the edges if needed to keep the field of
209 view the same.

210 **Image processing and analysis**

211 *ECS volume fraction and widths*

212 SUSHI images are single sections taken from z-stacks or time-lapse series for Fig. 1B,
213 selected to match the x-y-z planes. Brightness and contrast were adjusted for each
214 individual image using ImageJ (NIH) and the look-up table (LUT) was 'grays'. To
215 measure the ECS volume fraction (VF) and widths, images were binarized using a
216 wavelet-based software SpineJ (Levet et al., 2020) (**Fig. 1A**). For the VF (α), we
217 computed the ratio of pixels representing ECS over the total number of pixels ($\alpha =$
218 $N_{\text{ECS}}/N_{\text{total}}$) in a region of interest. For ECS widths, we analyzed 3-pixel-wide line profiles
219 drawn across the binarized images.

220 *Measurements of astrocytic structures and dendritic spines*

221 Images of astrocytes and dendrites are shown as maximum intensity z-projections with
222 the LUT 'orange hot'. Areas of astrocytic cell bodies and main branches were measured
223 by drawing a contour line around the structures and calculating their surface areas in
224 ImageJ. The widths of astrocytic fine processes were measured on raw images in
225 ImageJ, using the 'Plot Line Profile' function after drawing a 3-pixel-wide straight line
226 across the structure of interest. 'Dendritic vacuoles' were visually identified and
227 quantified by counting them in the images acquired before and after PFA application.

228 Morphological parameters of dendritic spines were measured using the SpineJ
229 software. The software identifies the neck region and places lines that are orthogonal to
230 the neck axis at regular intervals of 75 nm. It calculates the FWHM of the neck
231 diameter, returning the minimum, maximum and median values for each analyzed
232 spine. We limited the morphology analysis to dendritic spines with clear neck and head
233 compartments, commonly referred to as mushroom spines.

234 **Experimental design and statistical analysis**

235 Statistical tests were performed using Graphpad Prism software. Normality tests were
236 performed to confirm data were normally distributed. Normally distributed data are
237 presented as mean with standard deviation, while non-normal data are presented as
238 median with interquartile range. Paired t-tests were performed for normally distributed
239 data and Wilcoxon tests for non-normally distributed data. The size and type of
240 individual samples, n, for given experiments is indicated and specified in the results
241 section and figure legends. Asterisks in figures indicate p values as follows: * $p < 0.05$,
242 ** $p < 0.01$, *** $p < 0.001$, **** $p < 0.0001$. Image analysis and statistical tests were
243 performed blind to the experimental condition.

244

245 **Results**

246 ***30 minutes of PFA fixation has no detectable effects on ECS volume fraction***

247 To assess whether chemical fixation using PFA has an effect on hippocampal ECS
248 structure, we established an experimental workflow that allowed us to compare the
249 same sample before and after PFA fixation in a paired manner (**Fig. 1A**). As a readout

250 of the ECS structure, we analyzed the volume fraction (α) and geometric widths of the
251 ECS. The volume fraction α is an important structural parameter of brain tissue
252 (Nicholson and Hrabetova, 2017), which is defined by the ratio of the ECS volume over
253 the total volume in a region of interest.

254 We performed time-lapse confocal shadow imaging at 5-minute intervals before and
255 during PFA application using Calcein to label the ACSF that the slices were maintained
256 in (**Fig. 1B**). The images were binarized using SpineJ software (Levet et al., 2020)
257 based on wavelet filtering, allowing us to calculate the ratio of the number of 'ECS
258 pixels' over the total number of pixels as an estimate of the volume fraction in a region
259 of interest. We found that 30 minutes of PFA incubation did not cause any significant
260 changes in the ECS volume fraction (**Fig. 1C**; $n_{\text{PFA}} = 6$; $p = 0.3962$; paired t-test).

261 This result was confirmed by shadow-imaging with 3D-STED (SUSHI) (**Fig. 1D & E**; $n =$
262 6 ; $p = 0.3066$; paired t-test), indicating that 30 minutes of PFA incubation has little impact
263 on the volume fraction of the ECS in organotypic hippocampal slices.

264 ***Prolonged PFA incubation introduces pronounced artifacts***

265 As brain slices are often maintained in fixative for more than one hour or even
266 overnight, we investigated the effects of longer incubation times on ECS structure (**Fig.**
267 **2A**). We maintained the slices for 90 minutes under PFA or normal ACSF conditions
268 and compared SUSHI images before and after this period. Even 90 minutes of PFA
269 fixation appeared to affect neither ECS volume fraction (**Fig. 2B** left; $n = 6$; $p > 0.05$;
270 Wilcoxon matched-pairs test) nor widths measured in line profiles of binarized images

271 using SpineJ (**Fig. 2C, D, E**; $n_{\text{ctrl}} = 12$ lines, $n_{\text{PFA}} = 16$ lines; $p_{\text{ctrl}} = 0.1281$; $p_{\text{PFA}} =$
272 0.7249 ; paired t-test).

273 However, after 90 minutes under PFA conditions we observed dye-free, cellular blebs in
274 the immediate vicinity of cell bodies (**Fig. 2A, C** white arrows; **Fig. 2B** right, $n_{\text{live}} = 6$,
275 $n_{\text{PFA}} = 6$; $p = 0.0043$; Mann-Whitney test).

276 Incubation for 180 minutes with PFA caused even more pronounced changes, such as
277 dye accumulation around cell bodies and dye permeation into the cells (**Fig. 2F**),
278 indicating that PFA by itself permeabilized cell membranes, even in the absence of
279 detergents, like Triton, that are typically used in immunofluorescence protocols for
280 antibodies to reach intracellular epitopes (Goldenthal et al., 1985). Indeed, after
281 overnight PFA incubation the extracellular dye had entered into the cells (**Fig. 2G**),
282 indicating disruption of cellular membranes. This made assessing the impact of PFA on
283 the ECS impossible, because the inside-outside contrast, which is required for the
284 shadow imaging approach, was lost. Thus, more than 90 minutes of PFA fixation
285 appears to seriously damage the integrity of cellular membranes.

286 ***90 minutes of PFA fixation does not affect the morphology of astrocytes***

287 In addition to the effects of PFA on ECS structure, we set out to determine the impact of
288 PFA fixation on different cell types. We first focused on astrocytes, whose morphology
289 is known to be very sensitive to environmental changes, such as osmotic challenges
290 (Arizono et al., 2021) and transcardial perfusion of fixatives (Korogod et al., 2015). In
291 order to label astrocytes, we micro-injected AAV-GFAP-Clover viral particles into
292 organotypic hippocampal slices. Confocal microscopy did not turn up any significant

293 changes in the size of the major branches and cell bodies of astrocytes after 90 minutes
294 of PFA fixation (**Fig. 3A, B**; $n_{\text{branches}} = 12$; $n_{\text{bodies}} = 11$; $p_{\text{branches}} = 0.0952$; $p_{\text{bodies}} =$
295 0.1322 ; paired t-test). Likewise, STED microscopy did not detect any significant
296 changes in the widths of astrocytic fine processes (**Fig. 3C, D**; $n_{\text{ctrl}} = 26$; $n_{\text{PFA}} = 28$; $p =$
297 0.9589 ; paired t-test). These results suggest that PFA incubation by itself has
298 surprisingly little impact on astrocytic morphology.

299 ***90 minutes of PFA fixation leads to changes in dendritic spine morphology***

300 Finally, we performed similar experiments with neurons by virally labeling them with
301 Citrine as fluorescent protein. Using STED microscopy, we imaged dendrites and
302 dendritic spines before and after 90 minutes of PFA fixation (**Fig. 4A**). Unlike astrocytes,
303 many neurons formed 'dendritic vacuoles' after exposure for 90 minutes to PFA, which
304 could be extracellular holes in the dendrites or intracellular vacuoles free of the
305 fluorescent label. As we did not observe any dye-filled holes in dendrites in SUSHI
306 images, these structures most likely reflect Citrine-free spaces formed by coalescing
307 intracellular organelles such as mitochondria. In control experiments, i.e., in the
308 absence of PFA, we rarely observed such structures (**Fig. 4B**; $n_{\text{ctrl}} = 23$, $n_{\text{PFA}} = 31$; $n =$
309 number of analyzed dendritic segments; $p = 0.0074$; Mann-Whitney test).

310 Quantitative analysis of dendritic spine morphology revealed that there were no
311 significant changes in spine neck lengths (**Fig. 4D**); however, spine head areas became
312 significantly smaller (**Fig. 4C, D**) and the median spine neck diameter (measured along
313 the length of the neck, see Methods for details) became wider after 90 minutes of PFA
314 treatment (**Fig. 4E, F**; $p_{\text{h.area}} = 0.0157$; $p_{\text{width}} < 0.0001$; Wilcoxon matched-pair test).
315 While this effect was statistically highly significant for the median neck diameter, it was

316 not for the thinnest parts of the spine necks (**Fig. 4F**; $p_{\text{width}} = 0.1565$; Wilcoxon matched-
317 pair test).

318 These results show that dendrites and spines are affected by PFA fixation, suggesting
319 that neurons are more sensitive than astrocytes to PFA treatment in organotypic brain
320 slices within the limits of the resolution of our STED imaging approach.

321

322 **Discussion**

323 In this study, we describe the impact of chemical fixation with buffered PFA on tissue
324 architecture in organotypic hippocampal slices, focusing on the ECS and cellular
325 morphology. Our SUSHI approach indicates that immersion of organotypic brain slices
326 in PFA up to 90 minutes does not affect ECS volume fraction and widths. Similarly,
327 STED imaging showed that astrocytic morphology remains unaffected by PFA even at
328 the level of the fine processes. However, subtle changes in spine morphology appeared
329 within these relatively brief applications of PFA.

330 Previous studies have shown that transcardial perfusion of PFA reduces ECS widths
331 (Thorne and Nicholson, 2006) and causes major ECS shrinkage and astrocytic swelling
332 (Korogod et al., 2015). The fact that our experiments did not reveal such changes
333 indicates that they were not a direct result of PFA by itself on the tissue, but rather a
334 consequence of the anomalies subsequent to transcardial PFA perfusion, such as
335 anoxia (Tao-Cheng et al., 2007), or dehydration. This is in line with the observation that
336 acute slices fixed either chemically or cryogenically did not appear different in terms of
337 tissue quality and ECS distribution (Korogod et al., 2015). Given the absence of major

338 remodeling of the ECS under our conditions, it is perhaps not surprising that the
339 astrocytes did not show any changes either, suggesting that their morphology and ECS
340 topology are closely linked (Korogod et al., 2015).

341 Transcardial fixation was also shown to impact the spatial and molecular organization of
342 synaptic vesicles (Maus et al., 2020). In the same vein, a recent study showed that PFA
343 affects the behavior of proteins in liquid–liquid phase separation experiments,
344 underscoring the importance of understanding better the artifacts induced by PFA
345 fixation (Irgen-Gioro et al., 2022).

346 PFA fixation over 90 minutes considerably disturbed membrane integrity as indicated by
347 the penetration of the extracellular dye into the cells, preventing us from acquiring
348 SUSHI images. The membrane permeabilization was accompanied with cellular
349 blebbing, which has already been observed in cell cultures (Zhao et al., 2014),
350 suggesting that this is a common effect of PFA. Immunofluorescence experiments with
351 and without membrane permeabilization showed that PFA permeabilizes the membrane
352 to an extent that an antibody can pass into the cells (data not shown). Such loss of
353 membrane integrity needs to be considered in experiments focused on membrane
354 proteins, including ion channels or surface receptors (Ichikawa et al., 2022), as well as
355 many intracellular proteins that are linked to these proteins, such as components of the
356 postsynaptic density (Chen et al., 2008). A loss of membrane integrity may thus distort
357 our view of the synapse.

358 90 minutes of PFA fixation also induced ‘dendritic vacuoles’, which were virtually absent
359 in control experiments. Morphometric analysis of dendritic spines revealed that PFA
360 application leads to wider spine necks, in line with previous findings, where spine necks

361 were 30% thinner in cryogenically than chemically fixed samples (Tamada et al., 2020).
362 While we did not see any changes in spine neck length, we observed slightly decreased
363 spine head sizes.

364 To summarize, the time-lapse super-resolution approach allowed us to compare the
365 same tissue sample at the nanoscale under live and fixed conditions. Whereas short-
366 lasting fixation (< 30 minutes) is largely innocuous to tissue structure, longer PFA
367 applications unmistakably lead to artifacts. However, as our study was carried out in an
368 artificial system (organotypic brain slices), we do not know what happens *in vivo*, where
369 other factors (e.g., anoxia) come into play. In principle, STED imaging *in vivo* (Pfeiffer et
370 al., 2018) during transcardial perfusion of fixatives could address this knowledge gap.

371 With the proliferation of super-resolution studies based on chemical fixation, it is crucial
372 to reveal the effects of chemical fixatives, ambient conditions (e.g., temperature) and
373 other sample preparation steps on the native molecular and structural organization of
374 the samples, in order to optimize fixation protocols (Whelan and Bell, 2015; Pereira et
375 al., 2019; Laporte et al., 2022). Single-molecule imaging, ideally in combination with
376 STED (Inavalli et al., 2019), could provide a very sensitive readout to check protein
377 arrangements and cell morphology in parallel, helping to determine effective and
378 practical solutions to increase the preservation of fixed cells and tissues and the fidelity
379 of their microscopic analysis.

380 Finally, our study also presents a case for the development and use of live-cell super-
381 resolution microscopy, delivering information on the natural and dynamically evolving
382 state of the biological system free of concerns over fixation artifacts of whatever
383 provenance.

384 **References**

- 385 Arizono M, Idziak A, Quici F, Nagerl UV (2023) Getting sharper: the brain under the spotlight of super-
386 resolution microscopy. *Trends Cell Biol* 33:148-161.
- 387 Arizono M, Inavalli V, Bancelin S, Fernandez-Monreal M, Nagerl UV (2021) Super-resolution shadow
388 imaging reveals local remodeling of astrocytic microstructures and brain extracellular space
389 after osmotic challenge. *Glia* 69:1605-1613.
- 390 Chen X, Winters C, Azzam R, Li X, Galbraith JA, Leapman RD, Reese TS (2008) Organization of the core
391 structure of the postsynaptic density. *Proc Natl Acad Sci U S A* 105:4453-4458.
- 392 Ebersold HR, Cordier JL, Luthy P (1981) Bacterial mesosomes: method dependent artifacts. *Arch*
393 *Microbiol* 130:19-22.
- 394 Fox CH, Johnson FB, Whiting J, Roller PP (1985) Formaldehyde fixation. *J Histochem Cytochem* 33:845-
395 853.
- 396 Gahwiler BH (1981) Organotypic monolayer cultures of nervous tissue. *J Neurosci Methods* 4:329-342.
- 397 Goldenthal KL, Hedman K, Chen JW, August JT, Willingham MC (1985) Postfixation detergent treatment
398 for immunofluorescence suppresses localization of some integral membrane proteins. *J*
399 *Histochem Cytochem* 33:813-820.
- 400 Ichikawa T, Wang D, Miyazawa K, Miyata K, Oshima M, Fukuma T (2022) Chemical fixation creates
401 nanoscale clusters on the cell surface by aggregating membrane proteins. *Commun Biol* 5:487.
- 402 Inavalli V, Lenz MO, Butler C, Angibaud J, Compans B, Levet F, Tonnesen J, Rossier O, Giannone G,
403 Thoumine O, Hosy E, Choquet D, Sibarita JB, Nagerl UV (2019) A super-resolution platform for
404 correlative live single-molecule imaging and STED microscopy. *Nat Methods* 16:1263-1268.
- 405 Irgen-Giorgio S, Yoshida S, Walling V, Chong S (2022) Fixation can change the appearance of phase
406 separation in living cells. *Elife* 11.
- 407 Korogod N, Petersen CC, Knott GW (2015) Ultrastructural analysis of adult mouse neocortex comparing
408 aldehyde perfusion with cryo fixation. *Elife* 4.
- 409 Laporte MH, Klena N, Hamel V, Guichard P (2022) Visualizing the native cellular organization by coupling
410 cryofixation with expansion microscopy (Cryo-ExM). *Nat Methods* 19:216-222.
- 411 Levet F, Tonnesen J, Nagerl UV, Sibarita JB (2020) SpineJ: A software tool for quantitative analysis of
412 nanoscale spine morphology. *Methods* 174:49-55.
- 413 Maus L, Lee C, Altas B, Sertel SM, Weyand K, Rizzoli SO, Rhee J, Brose N, Imig C, Cooper BH (2020)
414 Ultrastructural Correlates of Presynaptic Functional Heterogeneity in Hippocampal Synapses.
415 *Cell Rep* 30:3632-3643 e3638.
- 416 Murk JL, Posthuma G, Koster AJ, Geuze HJ, Verkleij AJ, Kleijmeer MJ, Humbel BM (2003) Influence of
417 aldehyde fixation on the morphology of endosomes and lysosomes: quantitative analysis and
418 electron tomography. *J Microsc* 212:81-90.
- 419 Nicholson C, Hrabetova S (2017) Brain Extracellular Space: The Final Frontier of Neuroscience. *Biophys J*
420 113:2133-2142.
- 421 Pereira PM, Albrecht D, Culley S, Jacobs C, Marsh M, Mercer J, Henriques R (2019) Fix Your Membrane
422 Receptor Imaging: Actin Cytoskeleton and CD4 Membrane Organization Disruption by Chemical
423 Fixation. *Front Immunol* 10:675.
- 424 Pfeiffer T, Poll S, Bancelin S, Angibaud J, Inavalli VK, Keppler K, Mittag M, Fuhrmann M, Nagerl UV (2018)
425 Chronic 2P-STED imaging reveals high turnover of dendritic spines in the hippocampus in vivo.
426 *Elife* 7.
- 427 Ryter A (1988) Contribution of new cryomethods to a better knowledge of bacterial anatomy. *Ann Inst*
428 *Pasteur Microbiol* 139:33-44.

- 429 Schnell U, Dijk F, Sjollema KA, Giepmans BN (2012) Immunolabeling artifacts and the need for live-cell
430 imaging. *Nat Methods* 9:152-158.
- 431 Tamada H, Blanc J, Korogod N, Petersen CC, Knott GW (2020) Ultrastructural comparison of dendritic
432 spine morphology preserved with cryo and chemical fixation. *Elife* 9.
- 433 Tanaka KA, Suzuki KG, Shirai YM, Shibutani ST, Miyahara MS, Tsuboi H, Yahara M, Yoshimura A, Mayor S,
434 Fujiwara TK, Kusumi A (2010) Membrane molecules mobile even after chemical fixation. *Nat*
435 *Methods* 7:865-866.
- 436 Tao-Cheng JH, Gallant PE, Brightman MW, Dosemeci A, Reese TS (2007) Structural changes at synapses
437 after delayed perfusion fixation in different regions of the mouse brain. *J Comp Neurol* 501:731-
438 740.
- 439 Thorne RG, Nicholson C (2006) In vivo diffusion analysis with quantum dots and dextrans predicts the
440 width of brain extracellular space. *Proc Natl Acad Sci U S A* 103:5567-5572.
- 441 Tonnesen J, Inavalli V, Nagerl UV (2018) Super-Resolution Imaging of the Extracellular Space in Living
442 Brain Tissue. *Cell* 172:1108-1121 e1115.
- 443 Whelan DR, Bell TD (2015) Image artifacts in single molecule localization microscopy: why optimization
444 of sample preparation protocols matters. *Sci Rep* 5:7924.
- 445 Wyffels JT (2001) Principles and Techniques of Electron Microscopy: Biological Applications, Fourth
446 Edition, by M. A. Hayat. *Microsc Microanal* 7:66.
- 447 Zhao S, Liao H, Ao M, Wu L, Zhang X, Chen Y (2014) Fixation-induced cell blebbing on spread cells
448 inversely correlates with phosphatidylinositol 4,5-bisphosphate level in the plasma membrane.
449 *FEBS Open Bio* 4:190-199.
450

451 **Figure legends**

452 **Figure 1. Brief PFA incubation does not affect ECS volume fraction.**

453 **(A)** Graphical overview of the workflow of experiments and analysis. **(B)** Time-lapse
454 shadow imaging of ECS in live and buffered PFA conditions. The live condition is
455 represented both with a raw and inverted LUT. **(C)** ECS volume fraction α does not
456 change during 30 minutes incubation with PFA. The images were analyzed either as a
457 whole ('global') or divided into 'neuropil' or 'cell bodies' areas (n = 6). **(D)** Representative
458 images of ECS live and after 30 minutes of incubation with PFA. Blue squares indicate
459 the magnified area that is shown below with an inverted LUT. **(E)** Paired analysis of
460 ECS volume fraction live and after 30 minutes of incubation with PFA (n = 5; ns: not
461 significant; p < 0.05; in Wilcoxon matched-pairs test). Scale bars: 10 μ m.

462 **Figure 2. Prolonged PFA incubation introduces artifacts into ECS structure.**

463 **(A)** Representative images of ECS live and after 90 minutes of incubation with PFA.
464 The inset and white arrow indicate 'cell blebbing'. **(B) Left:** Paired analysis of ECS
465 volume fraction between live and 90 minutes after PFA fixation. The images were
466 analyzed either as a whole ('global') or divided into 'neuropil' or 'cell bodies' areas ($n_{\text{ctrl}} = 6$;
467 $n_{\text{PFA}} = 6$; ns: not significant; $p < 0.05$; in Wilcoxon matched-pairs test). **Right:**
468 Comparison of the 'cell blebbing' between live and 90 minutes PFA conditions ($n = 6$;
469 ns: not significant; $p < 0.05$; Mann-Whitney test). **(C)** Representative STED images of
470 ECS live and after 90 minutes of PFA fixation. **(D)** SUSHI-based analysis of ECS
471 widths. The blue lines indicate an example of the analyzed width. The line profiles are
472 shown together with measured FWHMs. **(E)** Paired analysis of ECS widths live and 90
473 minutes after PFA fixation ($n_{\text{ctrl}} = 12$; $n_{\text{PFA}} = 16$; ns: not significant; $p < 0.05$; paired t-
474 test). **(F)** Representative images of ECS live and 180 minutes after PFA fixation. Inset
475 and white arrows indicate examples of dye accumulation around cell bodies. **(G)** A
476 representative confocal shadow image after fixation overnight with PFA. Scale bars (A,
477 F, G): 10 μm ; (C, D): 5 μm .

478

479 **Figure 3. PFA fixation has no detectable effects on astrocytic fine structure. (A)**
480 Representative confocal images of a brain slice expressing GFAP-Clover in astrocytes,
481 live and 90 min after PFA fixation. White arrows indicate a representative astrocytic
482 main branch and cell body. **(B)** Paired analysis of astrocytic areas of main branches and
483 cell bodies live and 90 minutes after PFA fixation ($n_{\text{branches}} = 12$; $n_{\text{bodies}} = 11$; ns: not
484 significant; $p < 0.05$; paired t-test). **(C)** Representative STED images of astrocytic

485 structures in spongiform domain expressing GFAP-Clover, live and 90 min after PFA
486 fixation. The blue lines show representative line profiles of astrocytic structures to
487 determine their width. The line profiles are shown on the right together with calculated
488 FWHMs. **(D)** Paired analysis of widths of astrocytic fine processes, live and 90 minutes
489 after PFA fixation ($n_{\text{ctrl}} = 26$; $n_{\text{PFA}} = 28$; ns: not significant; $p < 0.05$; paired t-test). Scale
490 bars: 10 μm .

491

492 **Figure 4. PFA fixation affects spine morphology.**

493 **(A)** Representative STED maximum intensity z-projections of a dendritic segment
494 cytosolically filled with Citrine, live and 90 minutes after PFA fixation. White arrow
495 indicates a 'dendritic vacuole'. **(B)** Bar graph showing appearance of 'dendritic vacuoles'
496 after 90 minutes under live or fixed conditions (expressed as appearances over total
497 number of experiments: control: 2 out of 23; PFA: 15 out of 31; Mann-Whitney test). **(C)**
498 Representative STED images of dendritic spines and an example of head and neck
499 analysis using SpineJ. **(D)** Paired analysis of spine head area and neck length ($n_{\text{ctrl}} =$
500 79 ; $n_{\text{PFA}} = 86$; ns: not significant; $p < 0.05$; Wilcoxon matched-pairs test). **(E)** An example
501 of a dendritic spine with a wider neck after 90 minutes of PFA fixation. **(F)** Paired
502 analysis of spine neck width (smallest and median values) between live and 90 min
503 PFA-fixed conditions ($n_{\text{ctrl}} = 79$; $n_{\text{PFA}} = 86$; ns: not significant; $*p < 0.05$; $***p < 0.001$;
504 Wilcoxon matched-pairs test). Scale bars (A): 10 μm ; (C, E): 500 nm.

505

506 **Table. PFA fixation-induced effects on brain tissue microstructure.** Summary of
507 observed changes in various tissue structures (ECS, astrocytes and dendrites) for
508 different fixation times. VF: volume fraction; NE: not examined.

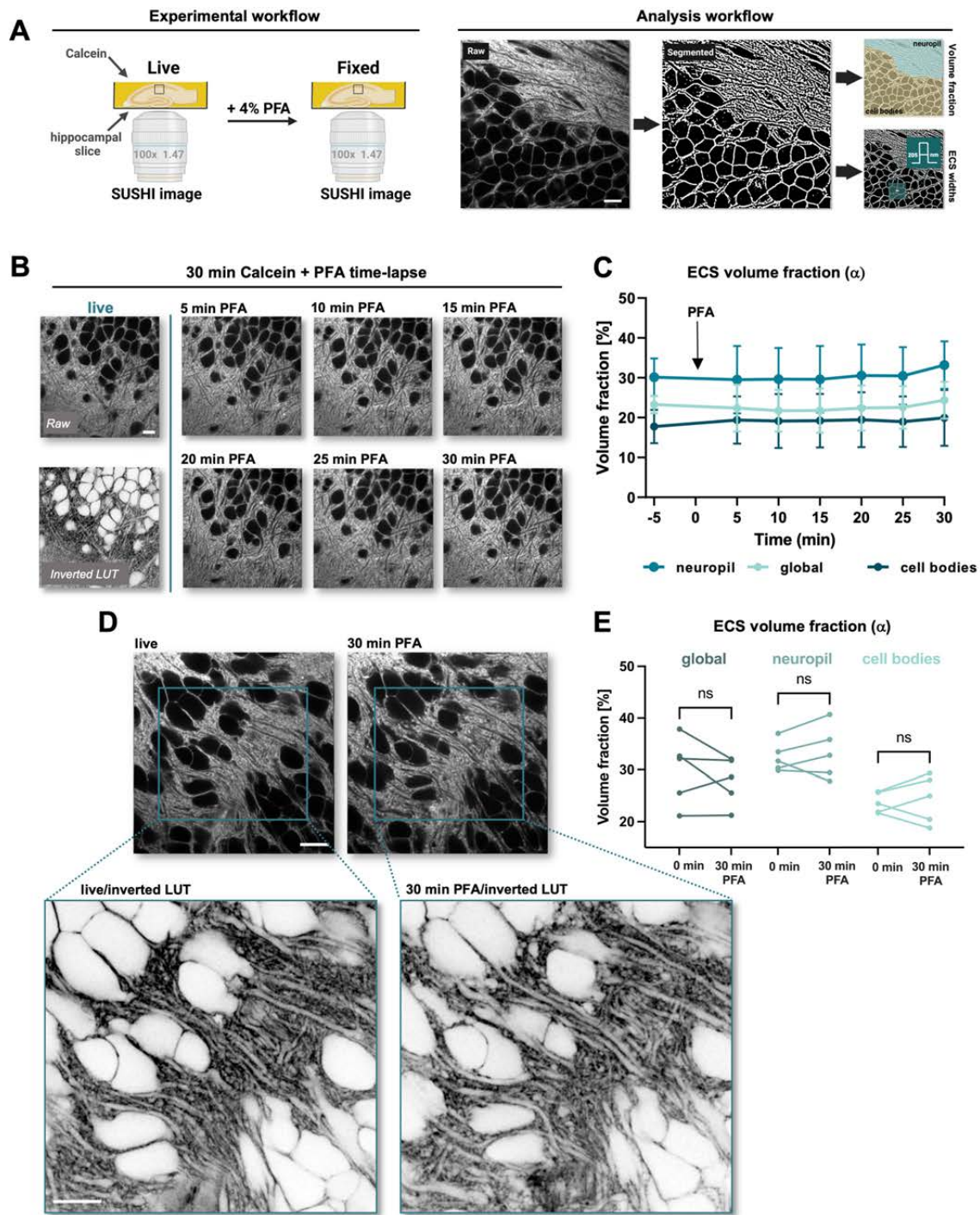


Figure 1

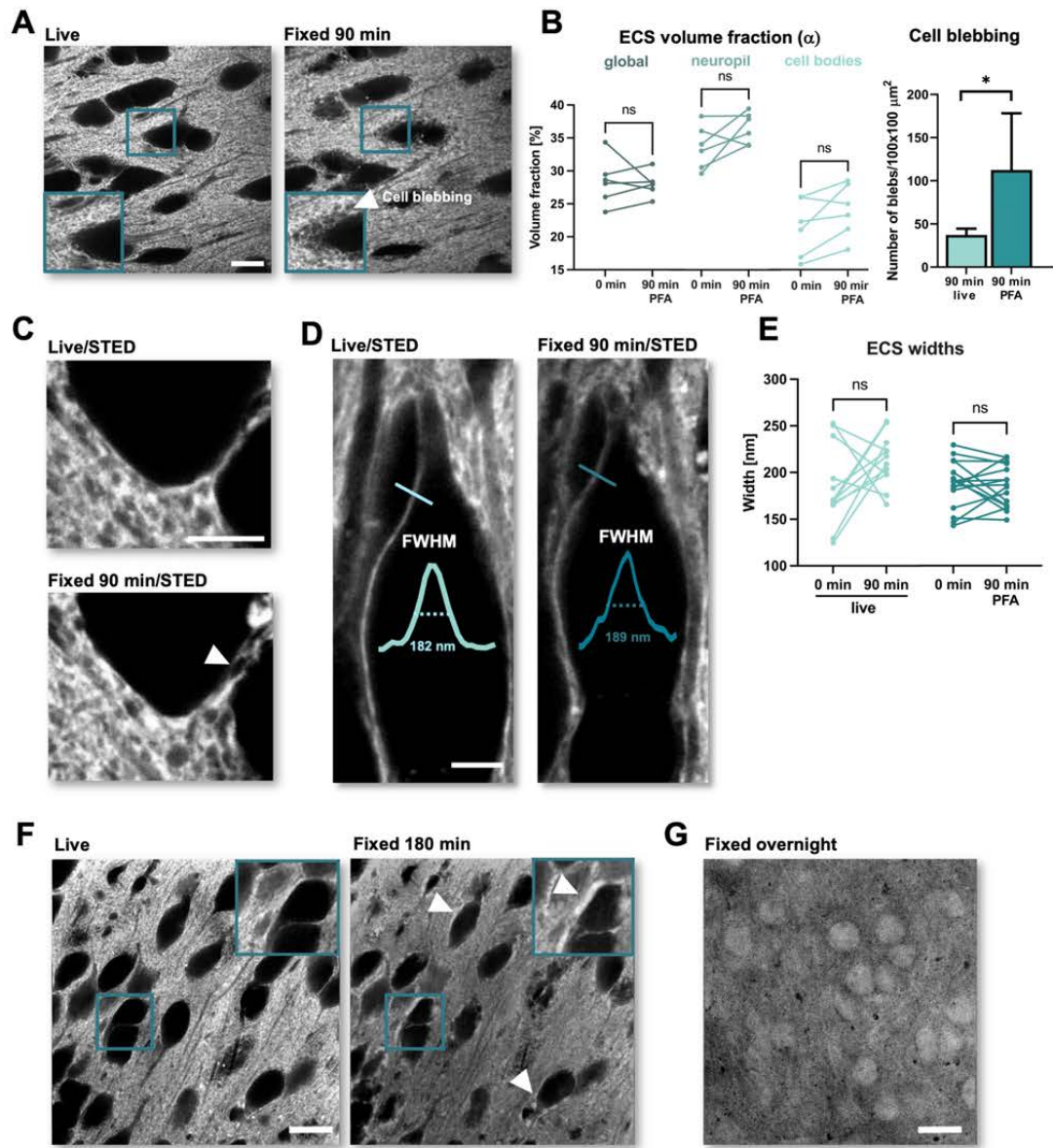


Figure 2

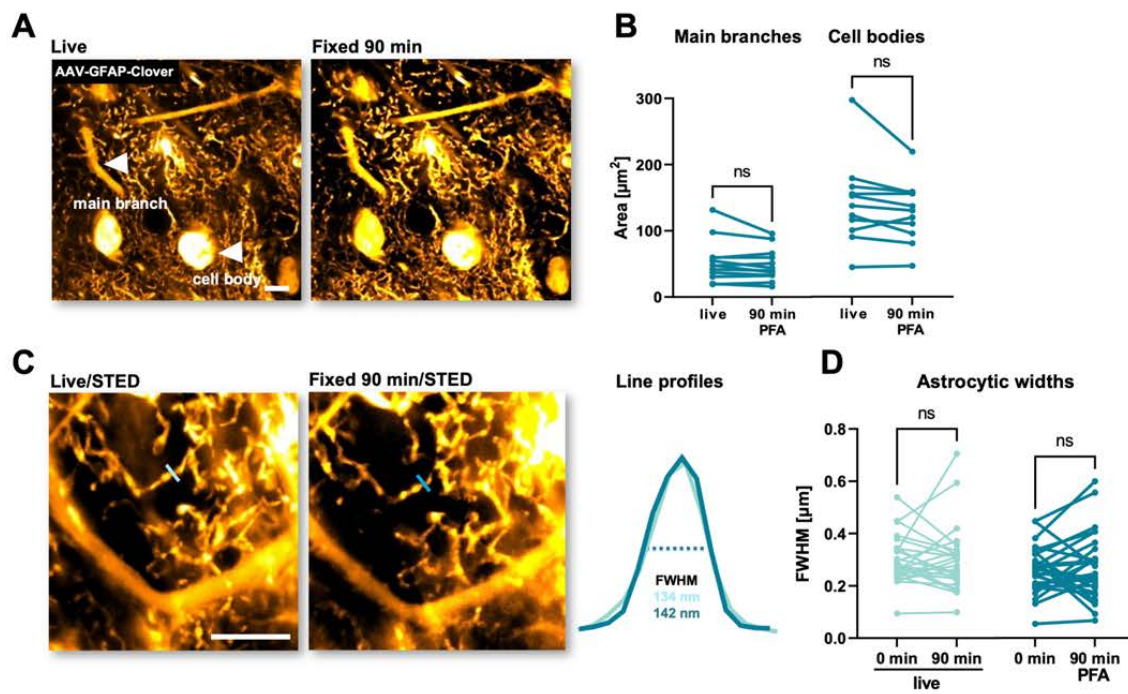


Figure 3

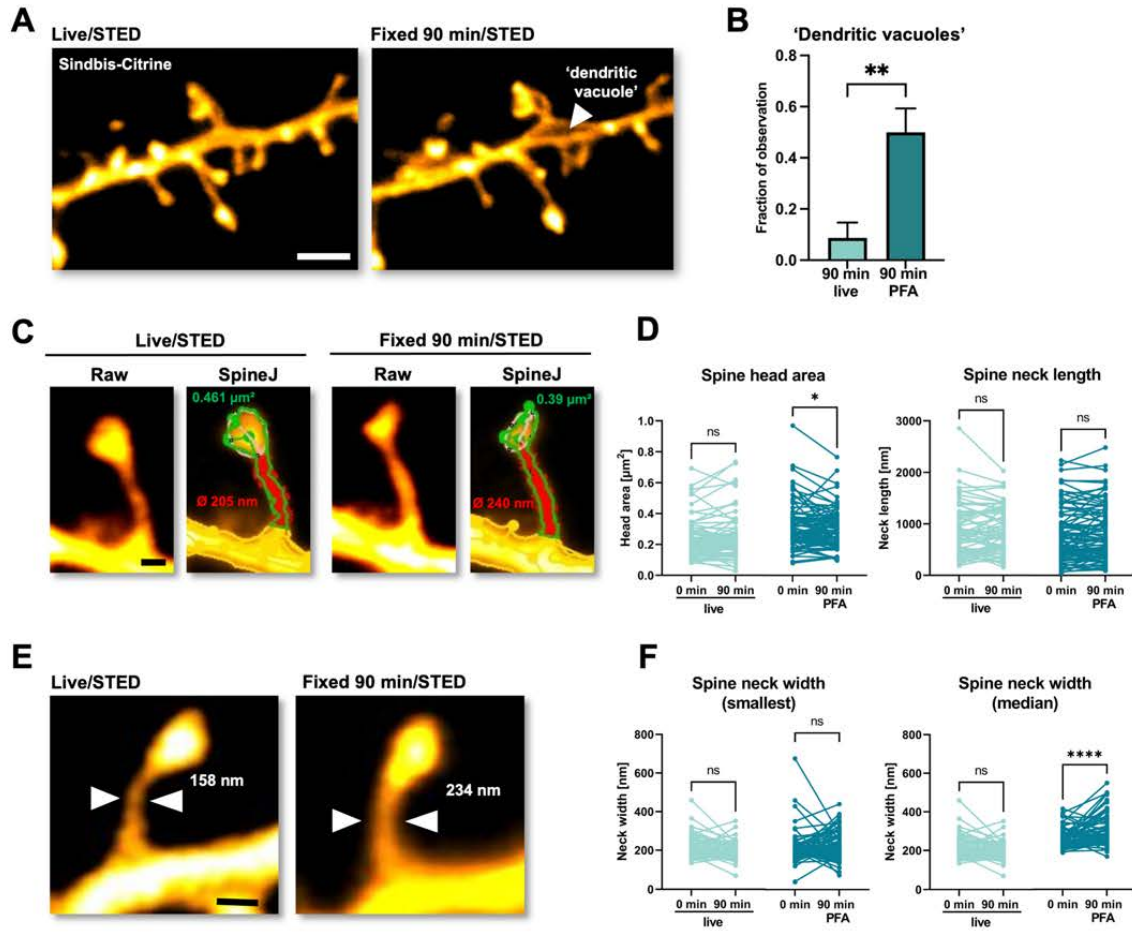


Figure 4

Structure \ Time of fixation	30 minutes	90 minutes	> 90 minutes
Extracellular space	No change in VF	No change in VF No change in width	NE (dye uptake)
Global tissue	No visible changes	Cell blebbing	Membrane permeabilization
Astrocytes	NE	No changes in areas of cell bodies and main branches No changes in widths of fine processes	NE
Dendrites Dendritic spines	NE	'Dendritic vacuoles' No changes in spine neck length Decreased spine head area Increased spine neck width	NE